ELSEVIER

Journal of Power Sources 108 (2002) 74–85

JOURNAL OF POWER SOURCES

www.elsevier.com/locate/jpowsour

Effects of Lanthanium on corrosion of NiAl in molten carbonate

Sang-Hoon Lee, Jae-Woong Choi, Sung-Goon Kang*

Division of Materials Science and Engineering, Hanyang University, Seoul 133-791, South Korea

Received 19 June 2001; received in revised form 19 September 2001; accepted 15 December 2001

Abstract

Lanthanium is added to NiAl which is a promising coating material for the wet-seal area of the separator in molten carbonate fuel cells. The effect of lathanium on the corrosion of NiAl in molten carbonate is investigated. Lathanium is precipitated at the grain boundaries of NiAl and reduces the grain size by one-fifth to one-eighth when added above 1.0 at.% by arc-melting. Though precipitated lathanium shows reactive effects and slightly increases the adherence of the oxide layer in cyclic oxidation, the oxide layer is disrupted at the grain boundaries when corroded in molten carbonate salt for more than 100 h. This behaviour is due to the internal stress which results from the oxidation.

Keywords: Molten carbonate fuel cell; Separator; NiAl; Lanthanium; Corrosion

1. Introduction

The severe corrosion of stainless-steel when used as a separator material for molten carbonate fuel cells (MCFCs) is well known [1,2] and is one of the major problems to the solved for MCFCs to become commercial. Indeed, the corrosion of the wet-seal of the separator is the most serious problem for achieving maintenance-free operation for 40 000 h [3].

To prevent corrosion of the wet-seal area, aluminizing coating methods for AISI316L or 310S stainless-steel have been examined but encounter problems such as changes in the stainless-steel structure due to the high annealing temperature (above 1000 °C) and to the degradation of the adherence of the aluminised coating to the stainless-steel itself [4]. Al–Ni plated material has been reported to provide longer lifetime than Al-plated material for a large amount of Al in Al–Ni plated material is retained as an Al–Ni intermetallic compound under the $LiAlO_2$ layer. In contrast, the Al in Al-plated material tends to diffuse from the surface into the substrate. NiAl is the main compound of the Al–Ni plated coating and provides a sufficient supply of Al to the $LiAlO_2$ layer, which is the stable form of alumina in molten Li/K carbonate [5]. Thus, NiAl has been suggested and applied as a promising coating material for the separator [1,6,7]. Lowering of the heat-treatment temperature and increasing adherence of the NiAl coating by electroplated-Ni and sputtered-Al deposition has been demonstrated [8]. NiAl used as a high-temperature aerospace material has found many applications due to its high melting point (1640 °C), and to its excellent resistance to high-temperature oxidation and corrosion by alumina formation [9] In the case of long-term oxidation and corrosion at high temperature, buckling occurs due to stress in the oxidation coating and, finally, spallation of the coating [10]. NiAl also forms NiO which dissolves in molten carbonate and causes reduction of the current density by electrical shorting when corrosion is continued in molten carbonate. This has been noted [11] as one of the main factors that reduced cell output.

In this study, we add lanthanium which is one of the reactive elements (REs) that are well known to have many beneficial effects on the oxidation and corrosion of alloys [12–19]. The RE effects have been explained in terms of several mechanisms but are still not clearly understood. Studies on the effects of lanthanium on corrosion are relatively few compared with those of other REs; only a few investigations have reported the effects of lanthanium and lanthanium oxide on the oxidation resistance of some metals [20–22]. In another study [23], lanthanium was selected the metal component of the most promising ceramics for the wet-seal area. Thus, we have investigated the effects of lanthanium on the corrosion of NiAl in molten carbonate through immersion tests, potentiodynamic polarisation tests and cyclic oxidation, and have discussed how lanthanium may be used to improve the corrosion resistance of NiAl in molten carbonate.

* Corresponding author. Tel.: +82-2-2293-3508; fax: +82-2-2296-4560.
E-mail address: sgkang@hanyang.ac.kr (S.-G. Kang).

0378-7753/02/$ – see front matter
PII: S0378-7753(01)01081-3

2. Experimental

A schematic diagram of the experimental processes is presented in Fig. 1.

2.1. Preparation and pre-oxidation of specimens

Lanthanium powder was added at 0.1, 0.2, 0.5 and 1.0 at.% in NiAl, mixed with Ni and Al powders in glove-box filled with argon gas, compacted in a cylindrical mould and, arc-melted under an argon atmosphere for three times. The specimens were heat-treated at 800 °C for 100 h in a vacuum furnace to give homogenisation, then cut with dimensions of 1 cm × 1 cm × 1 cm, polished with #2000 empty papers, and finally micro-polished to give mirror-like surfaces. Formation of the NiAl compound in the specimens was confirmed by X-ray diffraction (XRD), inductively coupled plasma-atomic emission spectormetry (ICP-AES) results for the actual lanthanium composition in the alloys are presented in Table 1. The pre-oxidation layers were formed on these specimens through constant temperature heat-treatment at 800 °C for 2 h in an air atmosphere.

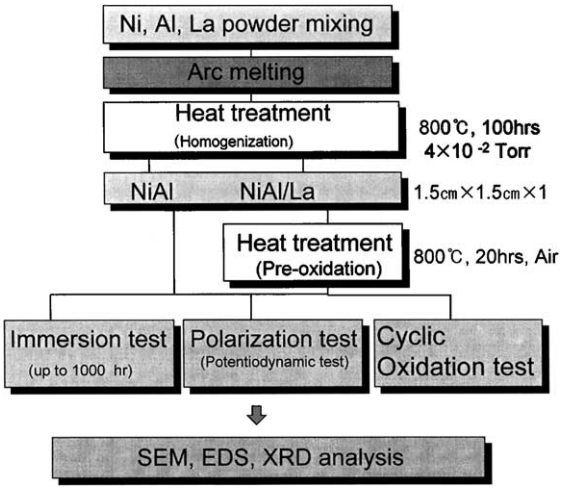

Fig. 1. Schematic diagram of experimental procedure.

Table 1
ICP-AES results of actual La composition (at.%) in Ni–Al–La specimen

Element	Specimen				
	NiAl	NiAl/0.1La	NiAl/0.2La	NiAl/0.5La	NiAl/1.0La
La	0	0.07	0.16	0.37	0.84

2.2. Cyclic oxidation test

To investigate the adherence and morphology of the oxidised layers of NiAl and NiAl/La, cyclic oxidation tests were performed. A schematic diagram of cyclic oxidation apparatus is shown in Fig. 2. This is composed of three components: (i) a horizontal furnace controlling the atmosphere and the temperature; (ii) a specimen holder moving specimens into the hot or cooling regions; (iii) a motor controller which controls the specimen holder. The temperature of the heating region was 800 °C and the cooling region was water-cooled. To simulate the gas atmosphere at the cathode of an actual MCFC stack, argon and air were controlled for the oxygen partial pressure to be 0.17 atm. The temperature–time schedule of one cycle is shown in Fig. 3. With this schedule, 100 cyclic oxidations were performed. The morphologies and compositions of the specimens were analysed by scanning electron microscopy (SEM) and energy dispersive X-ray spectroscopy (EDS).

2.3. Immersion test

Each specimen was immersed in the molten carbonate (62 mol% Li_2CO_3–38 mol% K_2CO_3) at 650 °C in a box furnace for up to 1000 h. The morphology, thickness, and composition, etc. of the corrosion product was analysed by SEM–EDS and XRD.

2.4. Electrochemical test

The high-temperature reference electrode used in this study was a mullite tube (o.d. 3/8 in., i.d. 1/4 in., length

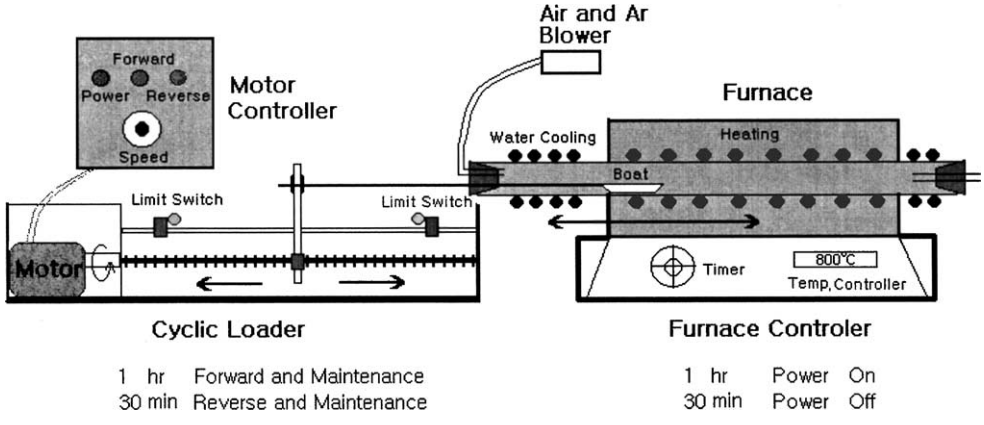

Fig. 2. Schematic diagram of experimental apparatus for cyclic oxidation test.

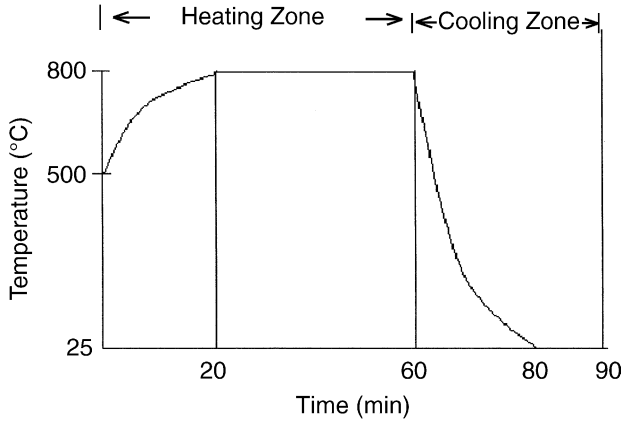

Fig. 3. Temperature–time history of a cyclic oxidation.

24 in.) of which one closed end was ground so as to act as mullite membrane through which sodium ions could migrate at high temperature.

The electrolyte was a eutectic liquid composed of 62 mol% Li_2CO_3–38 mol% K_2CO_3 which was melted in an alumina crucible at 650 °C. The gas supplied to the standard electrode was composed of CO_2 (1/3 atm) and O_2 (2/3 atm)and the flowing rate of the gas was 100 cm^3/min which was controlled precisely by a mass flow controller. A schematic diagram of the electrochemical experimental apparatus is shown in Fig. 4. Argon gas was blown into the chamber of the apparatus to create an inert atmosphere in the chamber during the polarisation test. When the temperature of the chamber reached 650 °C and the carbonate was molten, the working electrode was immersed. The potentiodynamic polarisation curve was performed at a rate of 1 mV s^{-1} after reaching the open-circuit potential (OCP). These processes were carried out with a Keithey model multimeter, an electrometer, and a PARC model 273 potentiostat that were controlled with personal computer.

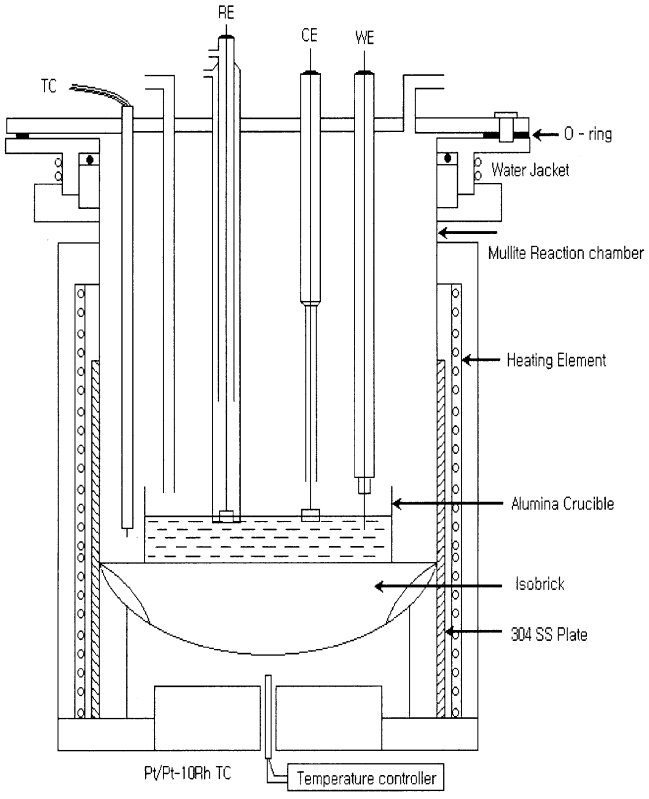

Fig. 4. Schematic diagram of experimental apparatus for analyses of electrochemical polarisation behaviour.

3. Results and discussion

3.1. NiAl and NiAl/La alloys

The XRD analysis of NiAl and NiAl/La specimens which were made by arc-melting and homogenization are presented in Fig. 5. With increasing lanthanium content, the peaks at lower 2θ values become more noticeable and this indicates that lanthanium has formed a new phase in NiAl. The SEM and EDS results of surface analyses are shown in

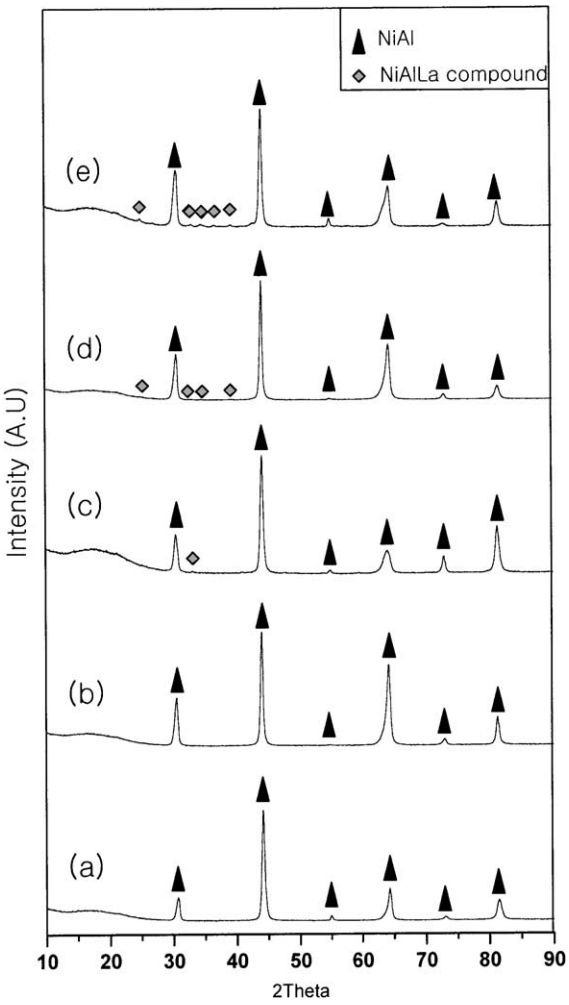

Fig. 5. XRD patterns of NiAl and NiAl/La alloys: (a) NiAl, (b) NiAl/0.1La, (c) NiAl/0.2La, (d) NiAl/0.5La, (e) NiAl/1.0La.

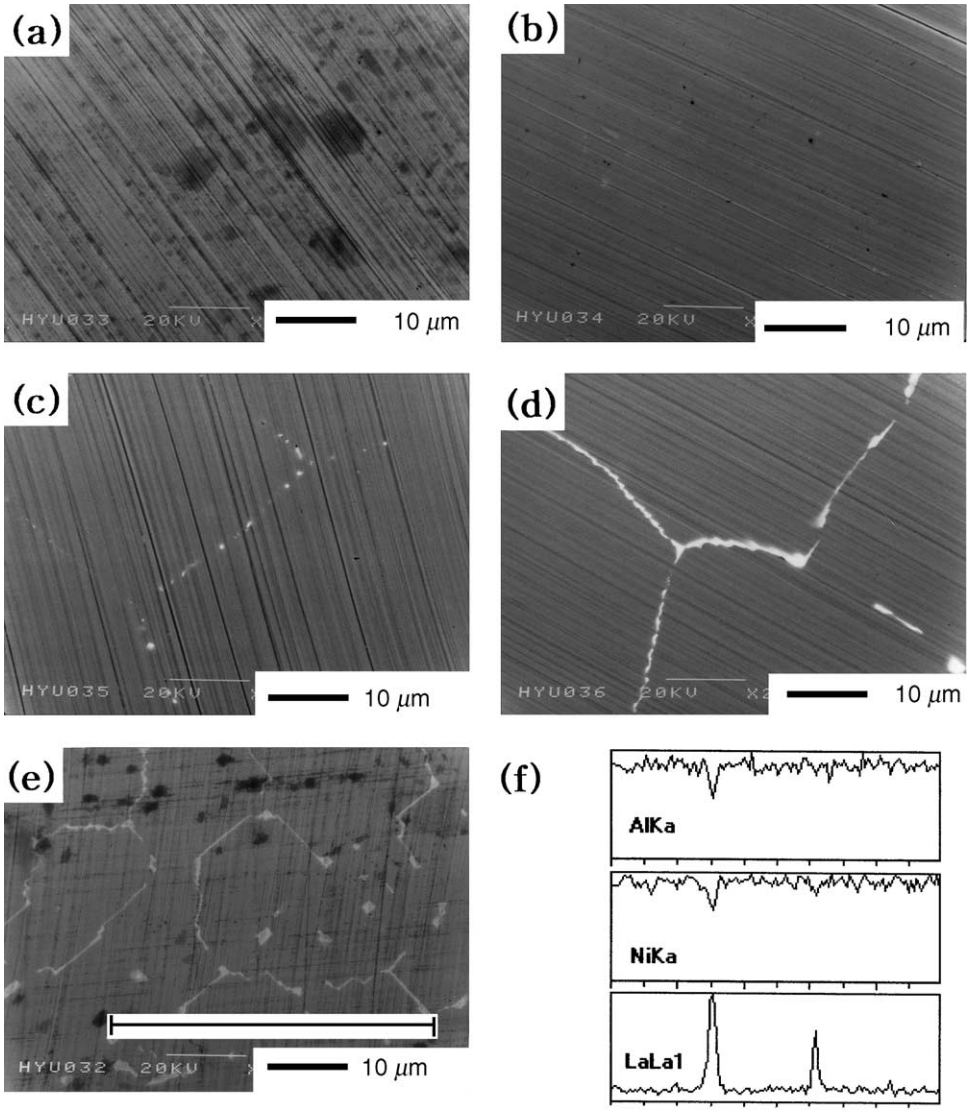

Fig. 6. SEM surface micrographs of specimens and EDS line-scanning profiles of NiAl/La alloy after micropolishing: (a) NiAl, (b) NiA/10.1La, (c) NiAl/0.2La, (d) NiAl/0.5La, (e) NiAl/1.0La, (f) line scan of (e).

Fig. 6. It can be seen in Fig. 6b–e that precipitates are located at grain boundaries in the NiAl and thicken as the lanthanium content is increased. When the lanthanium powder content is 1.0 wt.%, the grain size is reduced to about 1/5–1/8. Thus, lanthanium addition can be said to act as a grain-size refiner.

EDS line scanning results of precipitates at grain boundaries and grains are shown in Fig. 7. The spectra indicate that lanthanium is not dissolved inside the NiAl grains. Most of the lanthanium is precipitated at the grain boundary in the form of a Ni–Al–La compound for which the EDS peak intensity ratio of nickel, aluminum and lanthanium is about 1:1:1. The very low solubility of lanthanium in NiAl is due to the large differences in atomic radius. The atomic radius of lanthanium is 0.103 nm, i.e. about twice that of Al, 0.054 and Ni, 0.056 nm [24]. This large differences in atomic radius will cause very great internal strain and stress when lanthanium is precipitated in the NiAl lattice for which the ordering energy is very large and the intrinsic disorder parameter is less than 5×10^{-3} [25]. XRD analysis of these precipitated compounds show low intensity that cannot be identified with an accurate chemical composition from the XRD data reported to date.

To form an oxide layer on the surface of alloys before various tests, the specimens were pre-oxidised at 800 °C for 20 h in an air atmosphere. The results of optical observation of the pre-oxidised specimens are shown in Fig. 8. Numerous studies on the oxidation of NiAl and effects of the third element addition have been performed, but the oxidation and diffusion mechanism of NiAl is not clearly understood compared with those of Ni_3Al due to the intrinsic defect of the B2 structure. These studies show that the oxidation of NiAl produces only Al_2O_3 and that the forms of Al_2O_3 vary according to the time and temperature of oxidation [26].

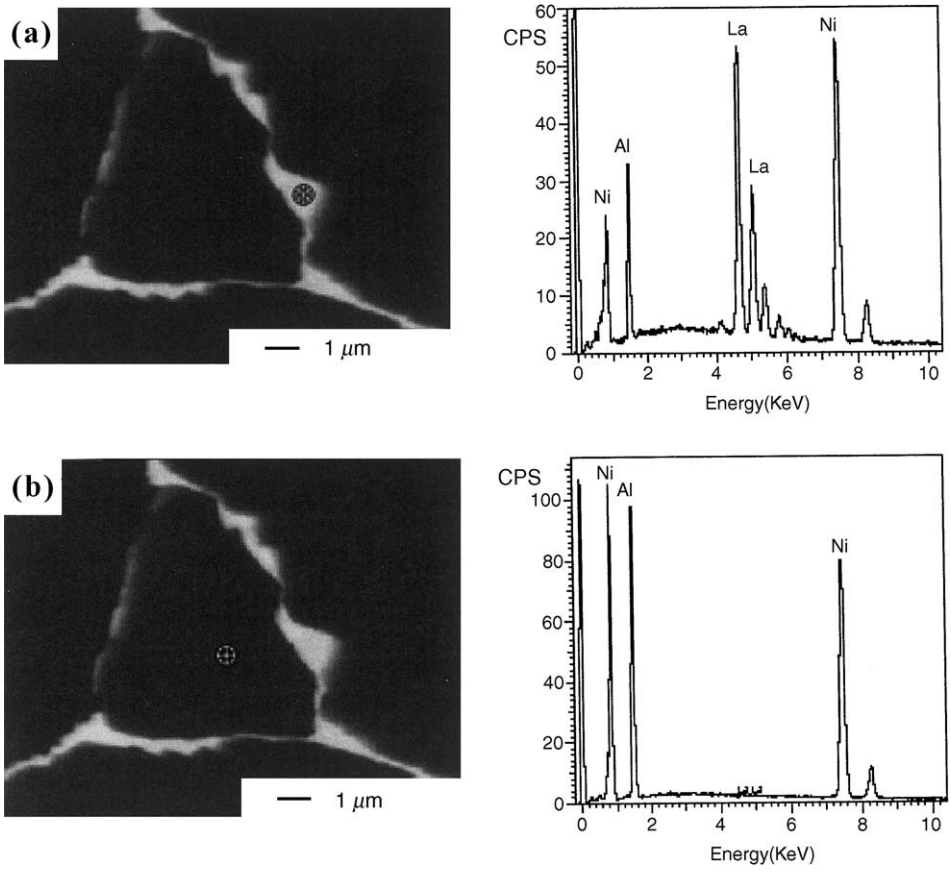

Fig. 7. SEM and EDS spectrum images of (a) boundary and (b) inner of a grain (×10 000).

Severe depletion of alumnium concentration does not occur up to 500 h of oxidation [27], and the stress evolution of alumina scale is observed over time [28]. The additions of the third element show changes in the alumina forms and have an effect on the oxidation rate of the oxide scale [29] and the stress evolution of the alumina scale [27].

The results of XRD, SEM and EDS mappings are presented in Figs. 9–11, respectively. The surface of the NiAl/1.0La specimen is oxidised to La_2O_3, Al_2O_3 and NiO. As can be seen in the EDS mapping results (Fig. 11), the Al_2O_3 layer is mainly formed on the grains, but double oxide layers, which consist of an outer Al_2O_3 layer and an inner La_2O_3 layer from oxidation of the Ni–Al–La compound are formed at the grain boundaries. This indicates indirectly that the oxidation of NiAl is proceeded by the diffusion of aluminum to the surface and the invasion of oxygen ions into the matrix. Thus, it can be concluded that Al_2O_3 is formed at the outermost layer of the grains by diffusion of aluminum to the surface, and, that La_2O_3 and Al_2O_3 for which the oxidation Gibbs free energies(ΔG_f) are quite large, are formed by the inner diffusion of oxygen ions along the grain boundaries. The Gibbs free energies of oxidation at 900 K are as follows [30]:

$$La_2O_3 \Delta G_f = -1535.174\,kJ/mol$$

$$Al_2O_3 \Delta G_f = -1393.83\,kJ/mol$$

$$NiO \Delta G_f = -157.929\,kJ/mol$$

As can be seen in the EDS mapping results of Fig. 11, the nickel content is drastically decreased at the grain boundaries during the oxidation of the Ni–Al–La compound. This suggests that lanthanium and aluminum are selectively oxidised due to their large Gibbs free energies of formation, so nickel is separated and diffuses into the grains. The thickness of the oxidised layers in Fig. 10 increases slightly as the lanthanium content is increased. It is considered that some lanthanium atoms in the matrix provide nucleation sites for oxidation and have high strain energy so that the oxidation is accelerated. In case of NiAl/0.5La and NiAl/1.0La, the oxide layers are found to bulge at the grain boundaries. When La_2O_3 is formed from the precipitated Ni–Al–La compound, the internal stress appears to arise from the differences in specific volume. In Fig. 11, the oxidation layer shows pegging effects, which are one of RE effects that have been known to increase the resistance to oxidation.

The EDS spectrum analyses in Fig. 12 show that the oxidation of precipitated Ni–Al–La compound forms lanthanium-rich oxide regions in the middle of the compound and aluminum-rich oxide regions at the boundary between the

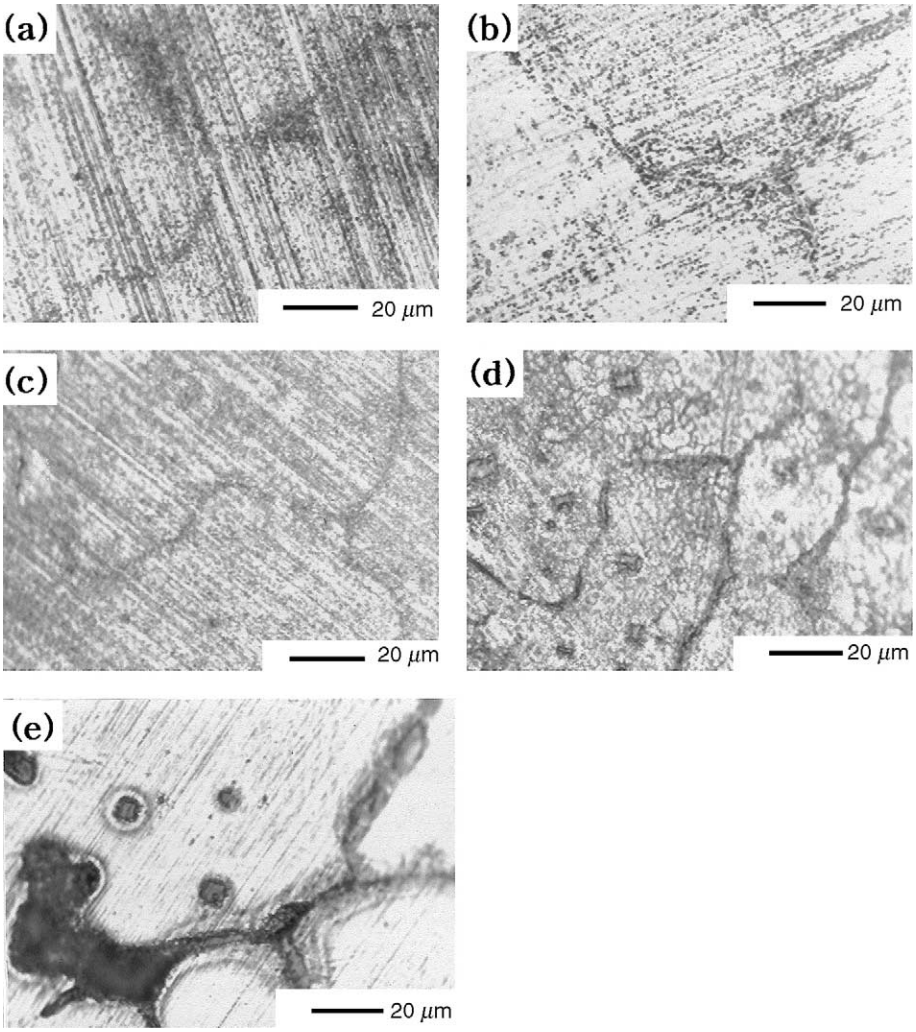

Fig. 8. Surface morphologies of pre-oxidised specimens in air atmosphere at 800 °C for 20 h: (a) NiAl, (b) NiAl/0.1La, (c) NiAl/0.2La, (d) NiAl/0.5La, (e)NiAl/1.0La.

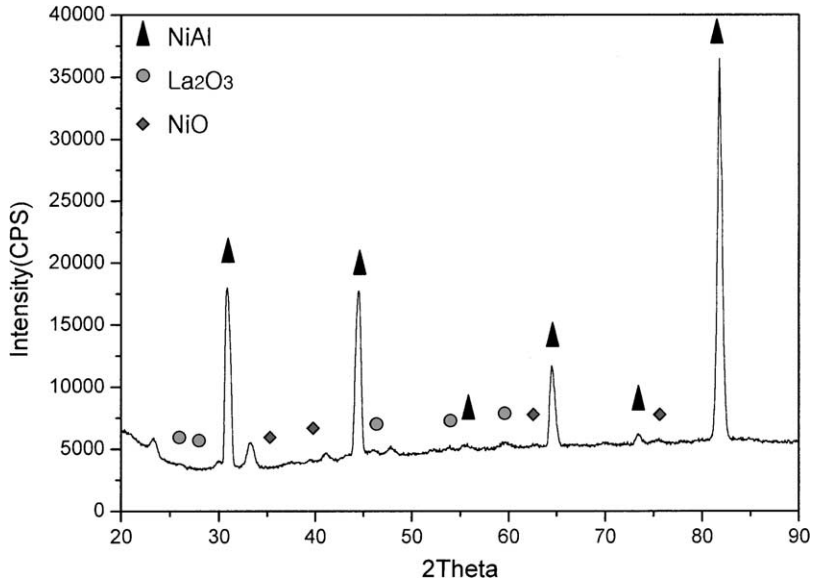

Fig. 9. XRD pattern of pre-oxidised NiAl/1.0La.

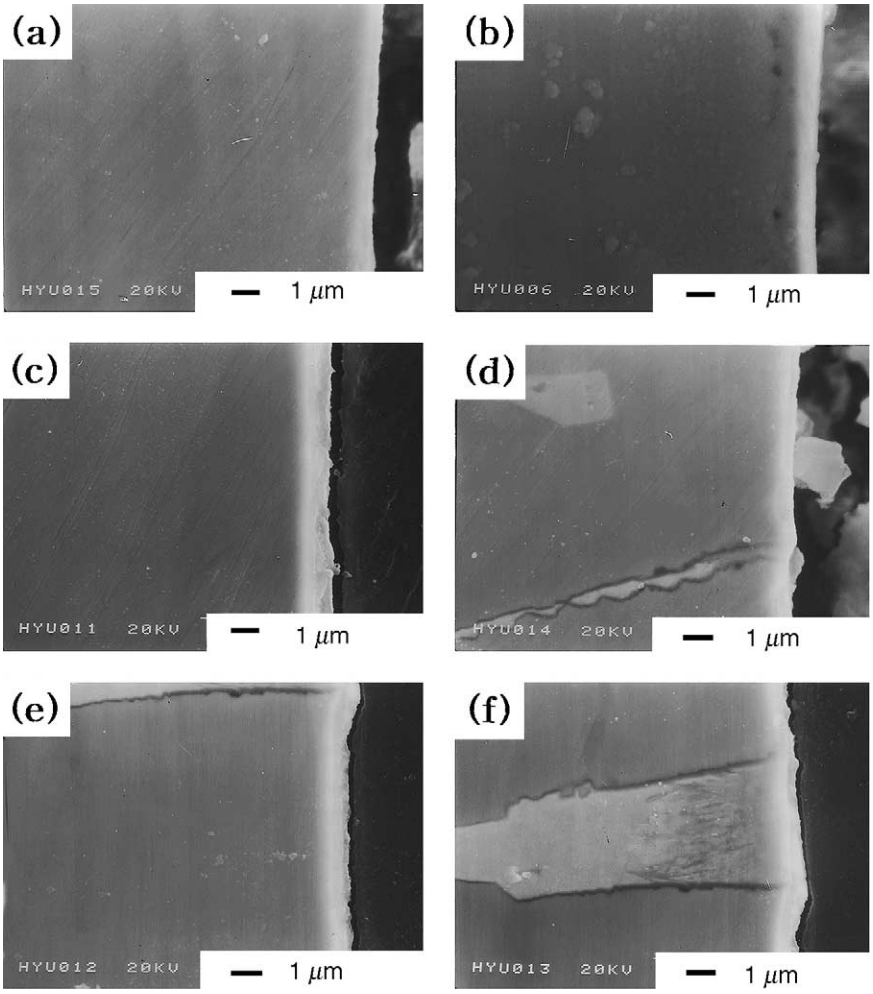

Fig. 10. Cross-sectional SEM images of pre-oxidised specimens: (a) NiAl, (b) NiAl/0.1La, (c) NiAl/0.2La, (d) NiAl/0.5La, (e) NiAl/1.0La, (f) grain boundary of NiAl/1.0La.

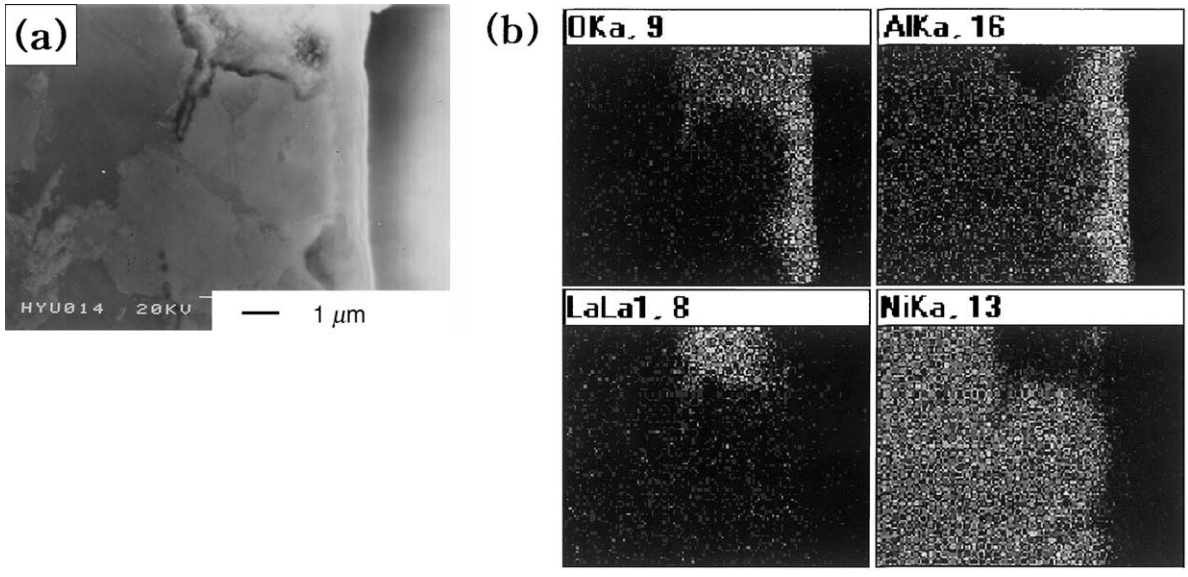

Fig. 11. (a) Cross-sectional SEM and (b) EDS mapping images of pre-oxidised NiAl/1.0La specimen at grain boundaries.

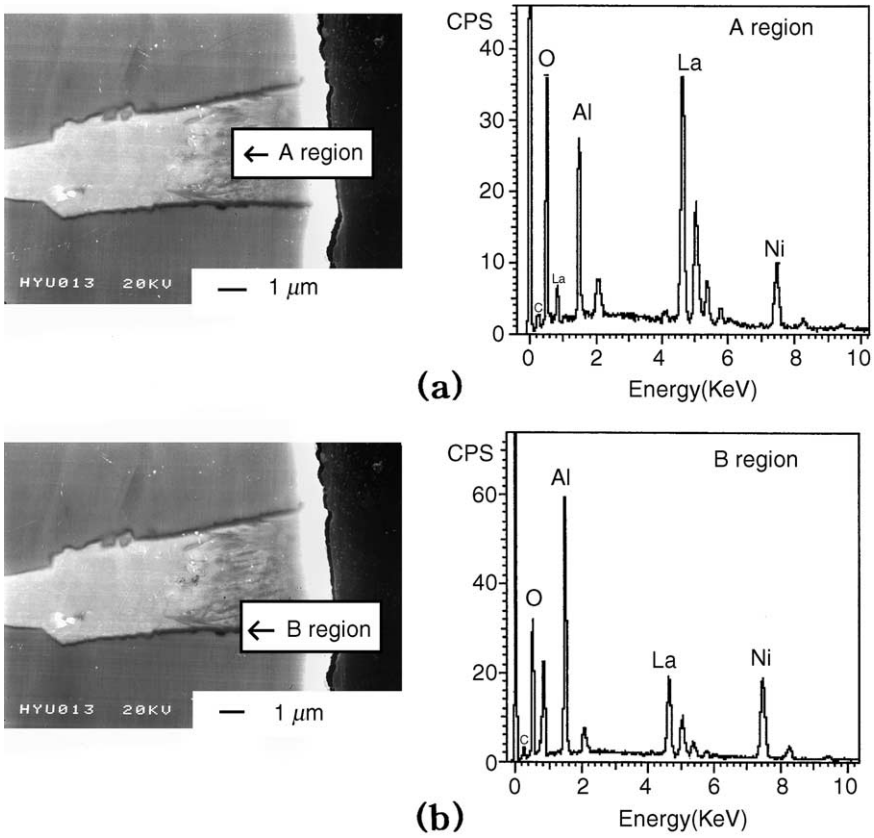

Fig. 12. Cross-sectional SEM and EDS analysis of pre-oxidised NiAl/1.0La specimen: (a) inner and (b) edge of precipitate.

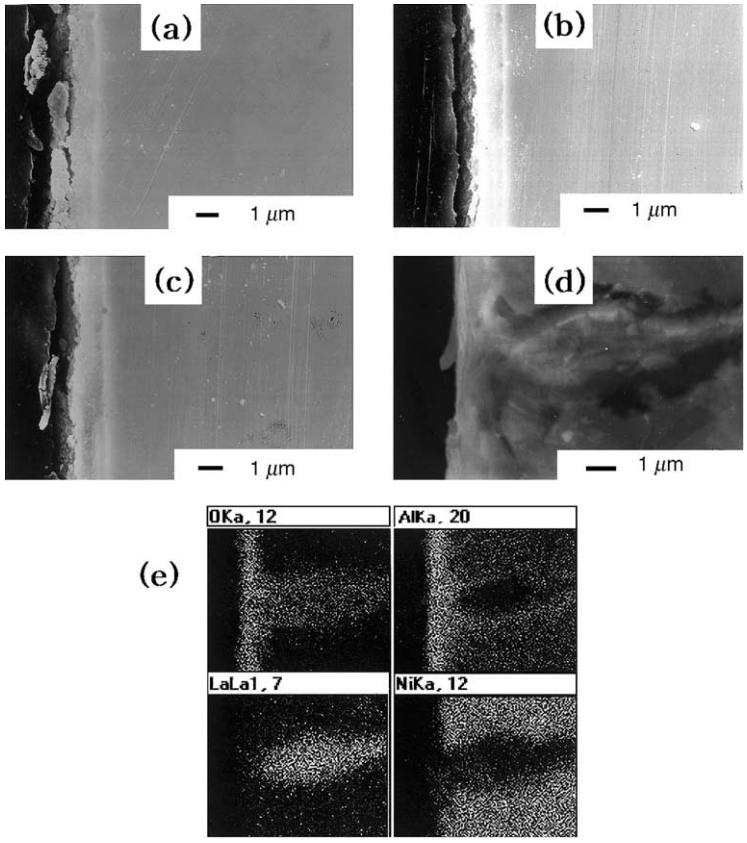

Fig. 13. Cross-sectional SEM images of specimens cyclic oxidised 100 times in air atmosphere at 800 °C: (a) NiAl, (b) NiAl/0.5La, (c) NiAl/1.0La, (d) grain boundary of NiAl/l.0La, (e) EDS mapping of (d).

compound and the grain. It is considered that aluminum diffuses from the grain and forms the aluminum-rich oxide region.

3.2. Cyclic oxidation test

SEM and EDS analyses of cyclic oxidation tests of pre-oxidised specimens are shown in Fig. 13. Compared with cyclic oxidised NiAl, NiAl/0.5La and NiAl/1.0La specimens have relatively less spalled parts of oxide layers, but do not show marked improvements in adherence, see Fig. 13. Both NiAl/0.5La (b) and NiAl/1.0La (c) also have a rough surface like NiAl (a) due to cyclic oxidation. SEM and EDS mapping analyses at grain boundaries are presented in Fig. 13d and e, which show the anchoring morphology of the oxide layer due to oxidation of Ni–Al–La compound along the grain boundary. So lanthanium addition appears to increase the oxidation resistance slightly in cyclic oxidation by so-called 'pegging effects'.

3.3. Immersion test

Results of 100 h immersion test for NiAl and NiAl/La alloys are presented in Fig. 14. From EDS analyses of the

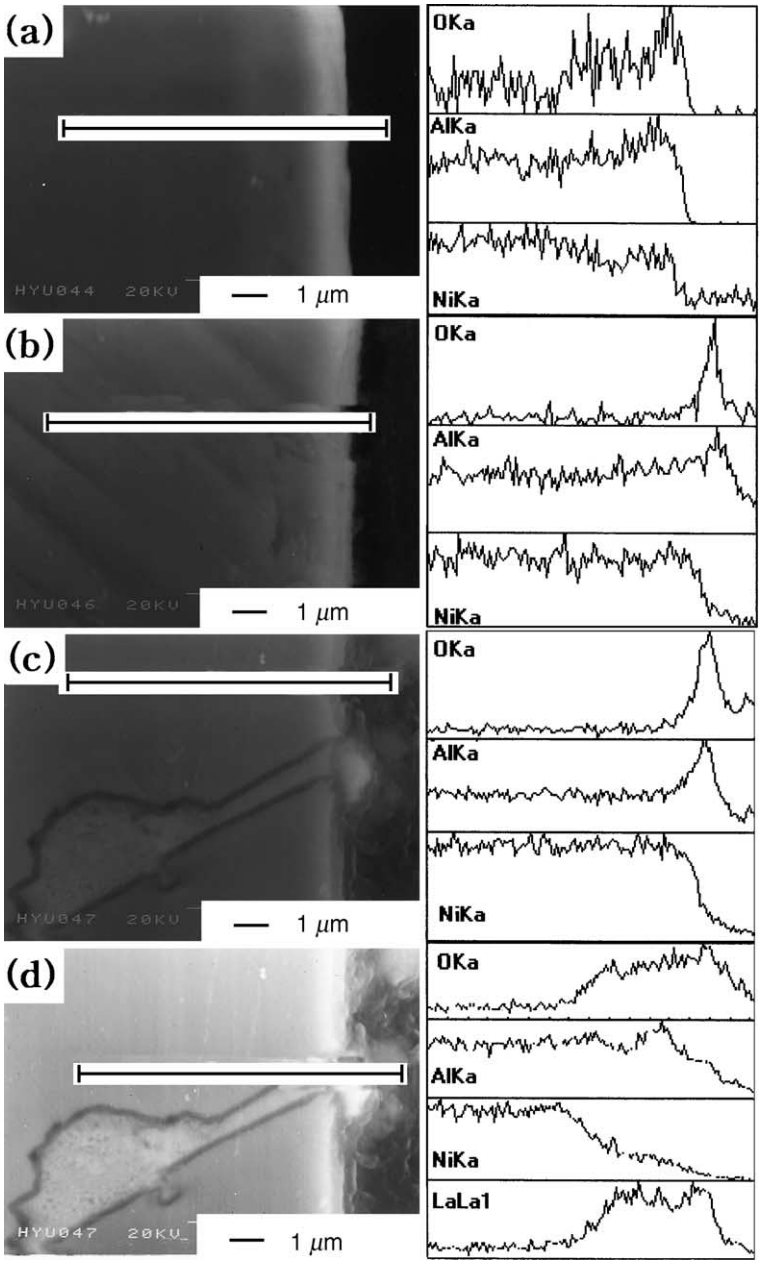

Fig. 14. Cross-sectional SEM and EDS images of specimens for 100 h in molten carbonate (62%Li_2CO_3–38%K_2CO_3) at 650 °C: (a) NiAl, (b) NiAl/0.5La, (c and d) NiAl/1.0La.

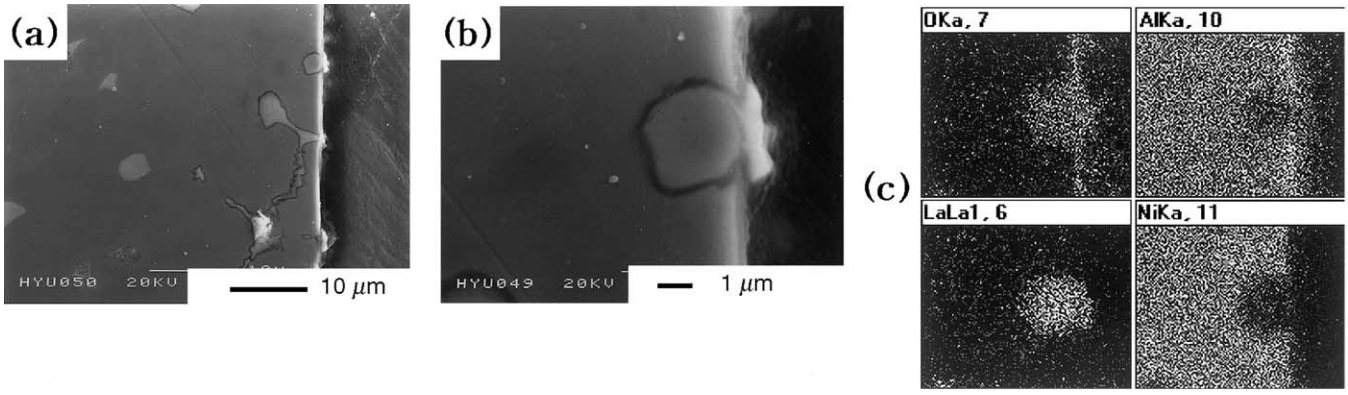

Fig. 15. (a) Cross-sectional SEM image of NiAl/1.0La corroded for 100 h in molten carbonate (62%Li_2CO_3–38%K_2CO_3) at 650 °C: (b) magnified SEM image of (a), (c) EDS mapping of (b).

corrosion products, the reactions are considered to be mainly expressed by the following equations [4].

$$M = M^{2+} + 2e^- \quad (1)$$

$$M + O_2{}^- = MO + 2e^- \quad (2)$$

$$M + 2OH^- = MO + H_2O + 2e^- \quad (3)$$

$$M + CO_2{}^{2-} = MO + CO_2 + 2e^- \quad (4)$$

As can be seen in Fig. 14c and d, the oxide layers are burst at the grain boundaries where precipitated lanthanium is oxidised. EDS analysis shows that the lanthanium oxide protudes from the precipitated Ni–Al–La compound. This is thought to be due to the internal stress which causes cracking of the oxide layer by the dissolution of NiO into molten carbonate because this protrusion does not appear in the previous 100 cycles of the oxidation test.

Another SEM analysis image of the NiAl/l.0La corroded for 100 h is shown in Fig. 15a. The burst parts at the oxidised surface can be seen clearly. The oxide layer formed on the grains is well-preserved, and the oxide layer only bursts where there is precipitated lanthanium oxide. Magnified

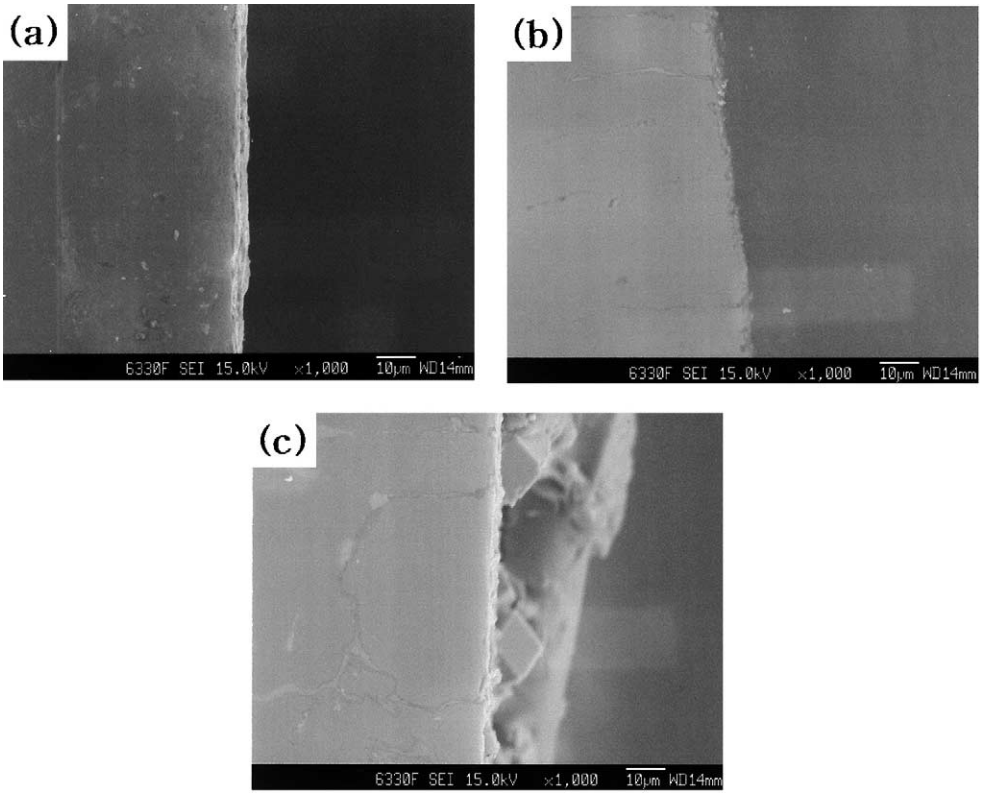

Fig. 16. Cross-sectional FE-SEM images of samples corroded for 1000 h in molten carbonate (62%Li_2CO_3–38%K_2CO_3) at 650 °C (×1000) (a) NiAl(PO) (b) NiAl/0.5La(PO) (c) NiAl/1.0La(PO); PO, pre-oxidised.

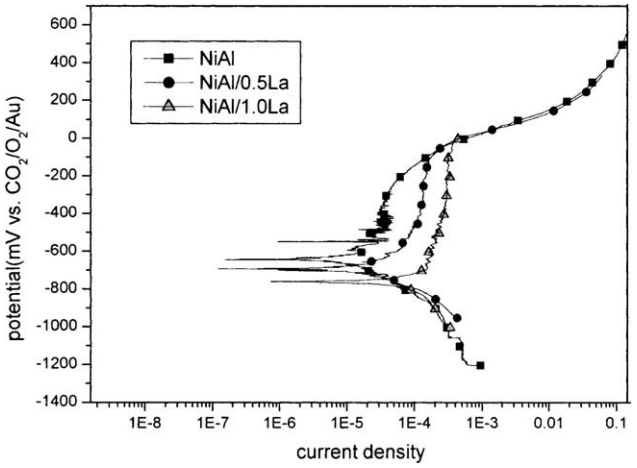

Fig. 17. Potentiodynamic behaviour of the specimens in molten carbonate salt at 650 °C.

SEM and EDS images given in Fig. 15b and c and show the burst-out morphology of the surface and composition. The $A1_2O_3$ layer is broken by the protruding, oxidised, lanthanium precipitate. Field emission SEM images of NiAl and NiAl/La alloys corroded for 100 h are presented in Fig. 16. In the case of NiAl (Fig. 16a),the pre-oxidised oxide layer is thickened, but both NiAl/0.5La (Fig. 16b) and NiAl/1.0La (Fig. 16c) have a spalled oxide layer and are internally oxidised along the grain boundary to about 20–30 μm for which the precipitate shows a dark line along the boundary.

3.4. Electrochemical test

Potentiodynamic polarization curves of NiAl, NiAl/0.5La and NiAl/1.0La alloys are given in Fig. 17. The OCPs of the specimens decrease from about −650 to −800 mV and the current densities increase in the range between −800 and 0 mV as lanthanium addition is increased. This is due to grain-size reduction, rapid oxidation of the Ni–Al–La compound at the grain boundary, and increasing oxidation rates of Al and Ni on the addition of lanthanium. These results indicate that the corrosion would proceed faster if the oxide layer is broken. This finding is in agreement with the results of the immersion test when the oxide layers of NiAl/0.5La and NiAl/1.0La burst out.

4. Conclusions

In the present study, the effects of lanthanium addition on the oxide layer of NiAl when corroded in molten carbonate are investigated. The following conclusions have been reached.

(i) Ni–Al–La compound is precipitated at the grain boundary when lanthanium is added to NiAl made when by arc-melting, and the grain size is reduced to about 1/5–1/8 when the initial lanthanium powder content is 1.0 at.%.

(ii) Addition of lanthanium increases the aluminum oxidation rate and thickens the oxide layer This improves the cyclic oxidation resistance slightly, and a pegging effect, one the RE effects, occurs at the grain boundary.

(iii) The oxide layer of La-added specimens consists of La_2O_3, Al_20_3 and NiO when oxidised at 800 °C in air, and the oxide layers are ‘bulb like’ at the grain boundary due to the internal stress set up by the volume differences of the oxides. These bulb layers burst when specimens corroded for more than 100 h in molten carbonate at 650 °C. Through these sites, internal oxidation and spallations of oxide layer proceed in the 1000 h immersion test.

(iv) Addition of lanthanium increases current densities and decreases the OCPs of the specimens. The decrease in grain size and the reactive precipitates at the grain boundary are considered to increase the current density in the electrochemical tests and the internal oxidation proceeds rapidly when the pre-oxidised layers are broken by the internal stress.

Therefore, though one of RE effects occurs and the Al oxidation rate is increased by lanthanium addition in cyclic oxidation, lanthanium does not show the anticipated effects of improving the corrosion resistance of NiAl in molten carbonate like other RE elements [6].

References

[1] J.P.P. Huijsmans, G.J. Kraaij, R.C. Makkus, G. Rietveld, E.F. Sitters, H.Th.J. Reijers, J. Power Sources 86 (2000) 117–121.
[2] A. Dicks, A. Siddle, J. Power Sources 86 (2000) 316–323.
[3] R.A. Donado, L.G. Marianowski, H.C. Maru, J. Electrochem. Soc. 131 (1984) 2538.
[4] J.E. Indacochea, I. Bloom, M. Krumpelt, J. Mater. Res. 13 (1998) 7.
[5] M. Murai, K. Takizawa, K. Soejima, H. Sotouchi, J. Electrochem. Soc. 143 (1996) 11.
[6] N. Fujimoto, M. Yamamoto, T. Nagaya, J. Power Sources 71 (1998) 23l–238.
[7] Y. Kawabata, N. Fujimoto, M. Yamamoto, T. Nagoya, M. Nishida, J. Power Sources A86 (2000) 324–328.
[8] E.R. Hwang, S.G. Kang, Korean J. Mater. Res. 7 (1997) 76.
[9] R.L. Mccarron, N.R. Lindblad, Corrosion 32 (1976) 476.
[10] M.W. Brumm, H.J. Grabke, Corrosion Sci. 34 (1993) 547.
[11] K. Tanimoto, M. Yanagida, T. Kojima, Y. Tamiya, H. Matsumoto, Y. Miyazaki, J. Power Sources 72 (1998) 77.
[12] C.T. Sims, N.S. Stoloff, W.C. Hagel, Superalloys II, Wiley, New York, Vol. 310, 1987.
[13] H.M. Tawancy, Metall. Trans. A 22A (1991) 1463.
[14] S.-C. Kung, V. Srinivasan, Oxid. Metals 33 (1990) 481.
[15] A.M. Huntz, Mater. Sci. Forum 43 (1989) 131.
[16] E. Schumann, J.C. Yang, Oxid. Metals 46 (1996) 37.
[17] L. Hanyi, W. Fuhui, Mater. Sci. Eng. A123 (1990) 123.
[18] H.G. Jung, K.Y. Kim, Oxid. Metals 46 (1996) 147.
[19] A.S. Khanna, C. Wasserfuhr, Mater. Sci. Eng. A 120 (1989) 185.
[20] X. Peng, D. Ping, T. Li, W. Wu, J. Electrochem. Soc. 145 (1998) 388.
[21] A.L. Rudd, Ca.B. Breslin, F. Mansfeld, Corrosion Sci. 42 (2000) 275–288.

[22] M.J. Capitan, S. Lefebvre, J.P. Dallas, J.L. Pastol, Surf. Coatings Tech. 100/101 (1998) 202–207.
[23] M. Keijzer, K. Hemmes, P.J.J.M. Van Der Put, J.H.W. De Wit, J. Schoonman, Corrosion Sci. 39 (1997) 483–494.
[24] R.D. Shannon, Acta Crystallogr. A32 (1976) 751.
[25] J.P. Neumann, Y.A. Chang, C.M. Lee, Acta Metall. 24 (1976) 593.
[26] M.W. Brumm, H.J. Grabke, Corrosion Sci. 33 (1992) 547.
[27] M. Bobeth, E. Bischoff, E. Scheumann, M. Rockstroh, M. Ruhle, Corrosion Sci. 37 (1995) 657–670.
[28] D.M. Lipkin, D.R. Clarke, M. Hollatz, M. Bobth, W. Pompe, Corrosion Sci. 39 (1997) 231–242.
[29] S. Taniguchi, T. Shibata, Oxid. Met. 25 (1986) 201.
[30] I. Barin, Thermochemical Data of Pure Substances, VCH, Weinheim, 1989.